Liquid Crystals
Publication details, including instructions for authors and subscription information:
http://www.informaworld.com/smpp/title~content=t713926090

Flow past finite obstacles in smectic liquid crystals: permeative flow induced S_A to S_C phase transition

H. G. Walton[a]; I. W. Stewart[b]; M. J. Towler[a]
[a] Sharp Laboratories of Europe Ltd, Oxford, UK [b] Department of Mathematics, University of Strathclyde, Glasgow, UK

To cite this Article Walton, H. G. , Stewart, I. W. and Towler, M. J.(1996) 'Flow past finite obstacles in smectic liquid crystals: permeative flow induced S_A to S_C phase transition', Liquid Crystals, 20: 5, 665 — 668
To link to this Article: DOI: 10.1080/02678299608031157
URL: http://dx.doi.org/10.1080/02678299608031157

LIQUID CRYSTALS, 1996, VOL. 20, NO. 5, 665–668

Preliminary communications

Flow past finite obstacles in smectic liquid crystals: permeative flow induced S_A to S_C phase transition

by H. G. WALTON, I. W. STEWART† and M. J. TOWLER*

Sharp Laboratories of Europe Ltd, Oxford Science Park, Oxford OX4 4GA, UK

†Department of Mathematics, University of Strathclyde, Glasgow G1 1XH, UK

(Received 8 February 1996; accepted 14 February 1996)

The hydrodynamic equations for flow past a finite barrier within a 'bookshelf' aligned smectic A liquid crystal are solved. Solutions are found for the flow components within (v_x) and normal (v_z) to the smectic layers. The behaviour of the v_z component is confirmed by experimental observation of both the buckling instability and a permeative flow induced S_A to S_C phase transition.

Smectic fluids have unusual hydrodynamic properties, flow within the layers being described by a Navier–Stokes like equation, whilst permeative flow across the layers is described by Darcy's law [1–4]. Flow past a semi-infinite barrier has previously been analysed [4, 5] and that past a finite barrier was approximated by the superposition of the boundary layers generated at each edge. As illustrated figuratively by de Gennes and Prost ([4] p. 444), we expect dilated and compressed regions either side of the barrier, together with parabolic boundary layers of width $4(\delta x)^{1/2}$ where $\delta = (\lambda_p \eta_3)^{1/2}$; λ_p is the permeation coefficient and η_3 (>0) is a viscosity coefficient ([4] p. 416).

Here we explicitly consider a finite rigid barrier of unit length centred at the origin in the xz-plane and lying along the vertical z-axis (figure 1). The smectic A layers are perpendicular to the barrier, but parallel to the direction of induced flow in the horizontal x-direction. By considering only the velocity components v_x and v_z in the xz-plane, the governing dynamic equations reduce to [4]

$$\frac{\partial P}{\partial z} = \frac{-v_z}{\lambda_p} \tag{1}$$

$$\frac{\partial P}{\partial x} = \eta_3 \frac{\partial^2 v_x}{\partial z^2} \tag{2}$$

$$\frac{\partial v_x}{\partial x} + \frac{\partial v_z}{\partial z} = 0 \tag{3}$$

where P is the pressure. We can introduce the stream

*Author for correspondence.

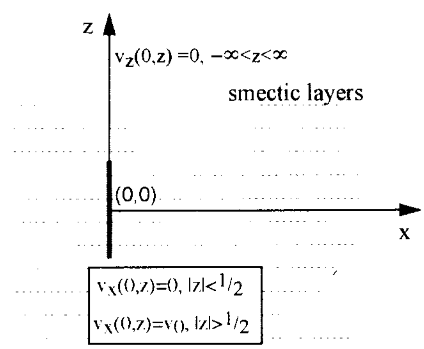

Figure 1. Schematic plan view of a finite barrier of unit length centred at the origin in the xz-plane and lying along the vertical z axis, perpendicular to the smectic layers.

function ψ such that

$$v_x = \frac{\partial \psi}{\partial z}, \quad v_z = -\frac{\partial \psi}{\partial x} \tag{4 a,b}$$

which allows us to eliminate P from equations (1) and (2) resulting in

$$\delta^2 \frac{\partial^4 \psi}{\partial z^4} - \frac{\partial^2 \psi}{\partial x^2} = 0. \tag{5}$$

The stream function ψ must satisfy the boundary conditions

$$v_x(0,z) = 0, |z| < \frac{1}{2}; \quad v_x(0,z) = v_0, |z| > \frac{1}{2} \tag{6}$$

$$v_z(0,z) = 0, \ -\infty < z < \infty \tag{7}$$

where v_0 is the magnitude of the flow in the x-direction at infinity where, of course, $v_z = 0$. The solution to equation (5) is then

$$\psi = \int_{-\infty}^{z} dz_1 \int_{-\infty}^{z_1} h(x, z_2)\, dz_2 + v_0 z \tag{8}$$

with

$$h(x,z) = \frac{v_0}{(\pi\delta|x|)^{1/2}} \sinh(z/4\delta|x|) \exp(-(z^2+\tfrac{1}{4})/4\delta|x|). \tag{9}$$

Notice that the sign of h changes with the sign of z. It is straight forward to verify that

$$\delta\frac{\partial^2 h}{\partial z^2} - \frac{\partial h}{\partial x} = 0 \tag{10}$$

$$\delta\frac{\partial^2 \psi}{\partial z^2} + \frac{\partial \psi}{\partial x} = 2\delta h \tag{11}$$

so that equation (5) is automatically satisfied: differentiate (11) separately with respect to z and x, subtract and substitute (10) as necessary. As $x \to 0$, $v_x \to v_0 S$ where $S(z)$ is a step function: $S=0$ for $|z|<\frac{1}{2}$, $S=1$ for $|z|>\frac{1}{2}$. Therefore the boundary conditions (6) are satisfied at $x=0$ for v_x. From equations (4 a), (8) and (9) we find that

$$v_x = v_0 - \frac{v_0}{2}\{\mathrm{erf}((z+\tfrac{1}{2})/2(\delta|x|)^{1/2}) - \mathrm{erf}((z-\tfrac{1}{2})/2(\delta|x|)^{1/2})\} \tag{12}$$

where erf is the usual error function. Further, inserting (8) into (4 b) and using the relation (11), it follows that

$$v_z = \pm \frac{v_0\delta^{1/2}}{(\pi|x|)^{1/2}} \sinh(z/4\delta|x|) \exp(-(z^2+\tfrac{1}{4})/4\delta|x|) \tag{13}$$

where the positive sign is taken for $x<0$ and the negative sign for $x>0$. Taking the limit as $x \to 0$, $v_z(0,z)=0$ for all z and hence the boundary condition (7) is satisfied. Further, $v_z(x,0)=0$ for all x. If $z \neq 0$ then

$$v_z(x,z)\begin{cases} <0 \text{ if } x>0 \text{ and } z>0 \text{ or } x<0 \text{ and } z<0, \\ >0 \text{ if } x>0 \text{ and } z<0 \text{ or } x<0 \text{ and } z>0. \end{cases} \tag{14}$$

Figure 2 illustrates the velocity field in the xz-plane where the direction and magnitude of the local velocity vectors are displayed for $x>0$. The experimental barrier (later) is 50 µm in diameter which we normalize to unity and approximate by a thin barrier at $x=0$, $|z|<\frac{1}{2}$. The approximation $\delta=0{\cdot}5$ µm is used for calculations ([1], p. 434), leading to a rescaled value of $\delta=0{\cdot}01$. Since the magnitude of the v_z component is generally small (away from $x=0$), we have exaggerated the v_z component by a factor of twenty-five to highlight the qualitative aspects of the solution provided by (12) and (13): this does not affect the basic features of the figure. Two parabolic boundary layers are seen to emanate from the z-axis at $z=\pm\frac{1}{2}$. From (9) these are of the form $(z\pm\frac{1}{2})^2=4\delta|x|$ and the relevant parts of these boundaries are plotted in figure 2. Outside the boundary layer $v_z \sim 0$ and, as

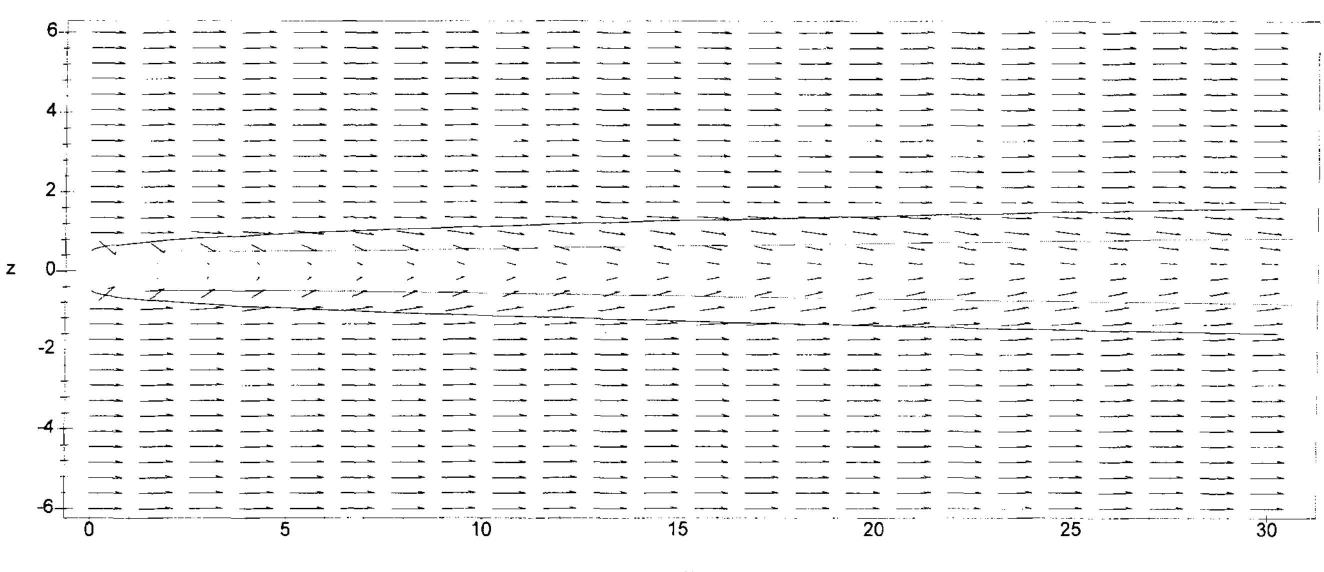

Figure 2. Calculated flow profile behind the barrier. Outer lines show a parabolic type boundary layer, outside of which the z-component of flow becomes small; inner lines show the condition for maximum z-component of velocity. These pairs of lines, respectively, define areas in which dilated and compressed regions may be expected.

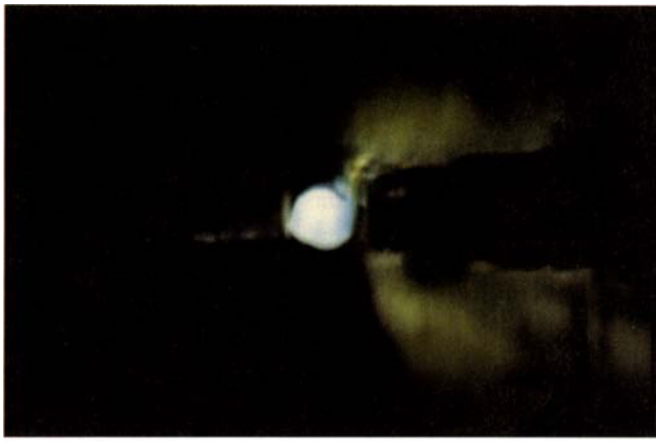

(*a*)

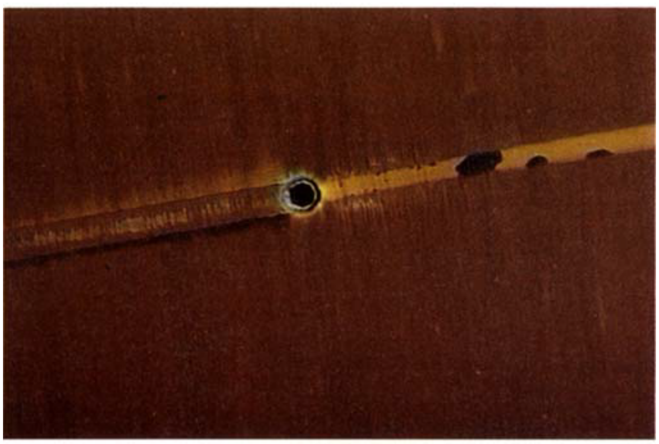

(*b*)

(*c*)

Figure 3. Response of smectic liquid crystal to a left–right flow past a cylindrical barrier, (*a*) $T \gg T_{AC}$, areas of undulation image the dilated regions before and after the barrier. (*b*) $T - T_{AC} = 0{\cdot}4$, areas of undulation and induced S_C phase image dilated and compressed regions. (*c*) $T - T_{AC} = 0{\cdot}2$, areas of induced S_C image compressed regions. The S_C domains also show flow alignment behaviour.

shown, only becomes significant inside the boundary layer. For $x > 0$ the maximum magnitude of v_z occurs when

$$x = \frac{z}{2\delta \ln\left(\dfrac{2z+1}{2z-1}\right)} \tag{15}$$

Equation (15) has real solutions only when $|z| > \frac{1}{2}$, and $x \to 0$ when $z \to \pm\frac{1}{2}$. Equation (15) is plotted in figure 2 and the resulting lines of course represent where the maximum magnitude of v_z actually occurs (z_{max}) for each value of $x > 0$. Consequently, behind the barrier, we may expect a compression of the layers from $z = 0$ to $z \approx z_{max}$, and a dilation from $z \approx z_{max}$ to $z = \pm(4\delta|x|)^{1/2} \pm \frac{1}{2}$, whilst in front of the barrier the region of dilation occurs from $z = 0$ to $z \approx z_{max}$.

Smectic A layers subjected to a dilation undergo a buckling instability [6] above a threshold which remains finite at all temperatures; layers subjected to a compressive stress undergo a S_A to S_C transition at a threshold which tends to zero as the temperature approaches T_{AC} (see figure 3 of [6]), but becomes very large above T_{AC}. The buckling instability has previously been used by Clark [7] to confirm the existence of the dilated regions when flowing past an air bubble in a cell filled with a liquid crystal in a S_A phase. Clearly if a material held near T_{AC} is used, then it should also be possible to image the compressed regions using the induced S_A to S_C phase transition, and confirm the behaviour expected from figure 2. To our knowledge the predicted regions of compression have not previously been experimentally imaged.

A 3 μm thick, parallel rubbed polyimide cell was fabricated with a photolithographically produced 50 μm diameter pillar at its centre and filled with the commercial material SCE8 (Cr < −20 S_C 58 S_A 78 N* 98 I). The cell thickness was decreased a far (negative) distance from the pillar and the consequences of the resultant flow past the obstacle were observed at different temperatures; this is shown in figure 3. Figure 3 (*a*) confirms Clark's observation of the dilation induced undulation instability for $T \gg T_{AC}$. Nearing T_{AC} both instabilities are seen (figure 3 (*b*)), with the oppositely directed $v_{x,z}$ gradients above and below the $z = 0$ line inducing S_C domains of differing flow birefringence. In addition, for $T \sim T_{AC}$ it is possible to induce purely the tilt instability (figure 3 (*c*)) for a small flow. Indeed, at $T = T_{AC}$ we expect zero threshold for the tilt instability and experimentally observe considerable fluctuations in birefringence of the sample behind the barrier, even without external attempts to induce flow. The form of the experimental findings show a striking similarity to the theoretical expectations of figure 2.

In summary we have extended the analysis of flow past obstacles in smectic liquid crystals to the case of finite barriers. The predicted dilated and compressed regions were experimentally confirmed by the observation of both the buckling instability and, for the first time, a permeative flow induced S_A to S_C phase transition. These results reiterate the importance of permeative effects in the hydrodynamic behaviour of smectic liquid crystals and provide tests of the predictive power of theoretical models. Future work will present exact calculations of the smectic layer displacement field for finite barriers and extend consideration to other smectic phases.

References

[1] Helfrich, W., 1969, *Phys. Rev. Lett.* **23,** 373.
[2] Martin, P. C., Parodi, O., and Pershan, P. S., 1972, *Phys. Rev. A.* **6,** 2401.
[3] Landau, L. D., and Lifschitz, E. M., 1986, *Theory of Elasticity*, 3rd Edn (Oxford: Pergamon Press).
[4] de Gennes, P. G., and Prost, J., 1993, *The Physics of Liquid Crystals*, 2nd Edn. (Oxford: Oxford University Press).
[5] de Gennes, P. G., 1974, *Phys. Fluids* **17,** 9.
[6] Ribotta, R., and Durand, G., 1977, *J. Phys., (Paris)* **38,** 179.
[7] Clark, N. A., 1978, *Phys. Rev. Lett.* **40,** 1663.